Inorg. Chem. **2004**, *43*, 2308–2317

Sandwich-Type Germanotungstates: Structure and Magnetic Properties of the Dimeric Polyoxoanions $[M_4(H_2O)_2(GeW_9O_{34})_2]^{12-}$ (M = Mn^{2+}, Cu^{2+}, Zn^{2+}, Cd^{2+})

Ulrich Kortz,*,† Saritha Nellutla,‡ Ashley C. Stowe,‡ Naresh S. Dalal,*,‡ Urs Rauwald,† Welbeck Danquah,† and Didier Ravot§

School of Engineering and Science, International University Bremen, P.O. Box 750 561, 28725 Bremen, Germany, Department of Chemistry and Biochemistry, Florida State University and National High Magnetic Field Laboratory and Center for Interdisciplinary Magnetic Resonance, Tallahassee, Florida 32306-4390, and Laboratoire de Physico-Chimie de la Matière Condensée, Université Montpellier II, case courrier 003, 34095 Montpellier Cedex 5, France

Received December 15, 2003

The novel dimeric germanotungstates $[M_4(H_2O)_2(GeW_9O_{34})_2]^{12-}$ (M = Mn^{2+}, Cu^{2+}, Zn^{2+}, Cd^{2+}) have been synthesized and characterized by IR spectroscopy, elemental analysis, magnetic measurements, and ^{183}W-NMR spectroscopy. X-ray single-crystal analyses were carried out on $Na_{12}[Mn_4(H_2O)_2(GeW_9O_{34})_2]\cdot 38H_2O$ (**Na_{12}-1**), which crystallizes in the monoclinic system, space group $P2_1/n$, with a = 13.0419(8) Å, b = 17.8422(10) Å, c = 21.1626(12) Å, β = 93.3120(10)°, and Z = 2; $Na_{11}Cs_2[Cu_4(H_2O)_2(GeW_9O_{34})_2]Cl\cdot 31H_2O$ (**Na_{11}Cs-2**) crystallizes in the triclinic system, space group $P\bar{1}$, with a = 12.2338(17) Å, b = 12.3833(17) Å, c = 15.449(2) Å, α = 100.041(2)°, β = 97.034(2)°, γ = 101.153(2)°, and Z = 1; $Na_{12}[Zn_4(H_2O)_2(GeW_9O_{34})_2]\cdot 32H_2O$ (**Na_{12}-3**) crystallizes in the triclinic system, space group $P\bar{1}$, with a = 11.589(3) Å, b = 12.811(3) Å, c = 17.221(4) Å, α = 97.828(6)°, β = 106.169(6)°, γ = 112.113(5)°, and Z = 1; $Na_{12}[Cd_4(H_2O)_2(GeW_9O_{34})_2]\cdot 32.2H_2O$ (**Na_{12}-4**) crystallizes also in the triclinic system, space group $P\bar{1}$, with a = 11.6923(17) Å, b = 12.8464(18) Å, c = 17.616(2) Å, α = 98.149(3)°, β = 105.677(3)°, γ = 112.233(2)°, and Z = 1. The polyanions consist of two lacunary B-α-$[GeW_9O_{34}]^{10-}$ Keggin moieties linked via a rhomblike M_4O_{16} (M = Mn, Cu, Zn, Cd) group leading to a sandwich-type structure. ^{183}W-NMR studies of the diamagnetic Zn and Cd derivatives indicate that the solid-state polyoxoanion structures are preserved in solution. EPR measurements on **Na_{12}-1** at frequencies up to 188 GHz and temperatures down to 4 K yield a single, exchange-narrowed peak, at g_{iso} = 1.9949, typical of Mn systems, and an upper limit of $|D|$ = 20.0 mT; its magnetization studies still await further theoretical treatment. Detailed EPR studies on **Na_{11}Cs-2** over temperatures down to 2 K and variable frequencies yield $g_{||}$ = 2.4303 and $g_{\perp}$ = 2.0567 and $A_{||}$ = 4.4 mT (delocalized over the Cu_4 framework), with $|D|$ = 12.1 mT. Magnetization studies in addition yield the exchange parameters J_1 = –11 and J_2 = –82 cm^{-1}, in agreement with the EPR studies.

Introduction

The class of polyoxometalates has been known since the time of Berzelius, but the first structure was determined by Keggin more than a century later.[1,2] This unique class of metal−oxygen clusters is composed of transition metals in groups V and VI (Mo, W, V, Nb, Ta) in a high oxidation state.[3,4] The metal centers are usually coordinated in a distorted octahedral fashion by oxygen atoms and the sharing of these octahedra by edges and corners leads to a large structural variety. Incorporation of one or more tetrahedral (e.g., PO_4), trigonal-pyramidal (e.g., AsO_3), or ditetrahedral (e.g., O_3POPO_3) hetero groups as additional building blocks

* Authors to whom correspondence should be addressed. E-mail: u.kortz@iu-bremen.de. Fax: +49-421-200 3229 (U.K.). E-mail: dalal@chemmail.chem.fsu.edu. Fax: 850-644-3398 (N.S.D.).
† International University Bremen.
‡ Florida State University.
§ Université Montpellier II.

(1) Berzelius, *J. Pogg. Ann.* **1826**, *6*, 369.
(2) (a) Keggin, J. F. *Nature* **1933**, *131*, 908. (b) Keggin, J. F. *Proc. R. Soc. A* **1934**, *144*, 75.
(3) Pope, M. T. *Heteropoly and Isopoly Oxometalates*; Springer-Verlag: Berlin, 1983.
(4) Pope, M. T.; Müller, A. *Angew. Chem., Int. Ed. Engl.* **1991**, *30*, 34.

10.1021/ic0354421 CCC: $27.50
Published on Web 03/12/2004

allows for further structural versatility. Mostly, the solid-state structure of polyoxometalates is preserved in solution and appropriate choice of the counterion allows for redissolution of a polyoxoanion in aqueous, organic, and mixed aqueous/organic solvents. Furthermore, polyoxoanions exhibit very high thermal stability in the solid state. In addition, substitution of one or more addenda atoms by redox-active transition metal ions (e.g., Fe^{3+}, Ru^{3+}) allows fine-tuning of the catalytic activity of polyoxoanions. These and other properties have led to increasing attention of this class of compounds worldwide. Applications of polyoxoanions include fields as diverse as catalysis, medicine, and magnetochemistry.[5−8]

At the same time it must be pointed out that the mechanism of formation of polyoxometalates is not well-understood and commonly described as self-assembly. Nevertheless, the synthesis of polyoxometalates is mostly rather simple and straightforward, once the proper reaction conditions have been identified.

Transition-metal-substituted polyoxometalates can also be of interest for their magnetic properties. Structures that contain more than one paramagnetic transition metal ion in close proximity may exhibit exchange-coupled spins leading to large spin ground states.[9,10] The polyoxometalate matrix may be considered a diamagnetic host encapsulating and thereby isolating magnetic clusters of transition metals.

Lacunary polyoxometalates are usually synthesized from complete precursor ions by loss of one or more MO_6 octahedra. Reaction of a stable, lacunary polyoxometalate with transition-metal ions usually leads to a product with the heteropolyanion framework unchanged. Depending upon the coordination requirement and the size of a given transition-metal ion, the geometry of the reaction product can therefore often be predicted.

Phosphotungstates and silicotungstates are probably the most intensively studied systems because they exhibit a large variety of lacunary precursor species that can usually be synthesized in one- or two-step procedures in high-yield (e.g., α-$PW_{11}O_{39}^{7-}$, γ-$PW_{10}O_{36}^{7-}$, *A*-$PW_9O_{34}^{9-}$, *B*-$PW_9O_{34}^{9-}$, $P_2W_{15}O_{56}^{12-}$, α-$SiW_{11}O_{39}^{8-}$, γ-$SiW_{10}O_{36}^{8-}$, and *A*-$SiW_9O_{34}^{10-}$).[3]

Sandwich-type polyoxometalates based on two *B*-α-$[XW_9O_{34}]^{n-}$ ($X = P^V$, As^V, Si^{IV}) or *B*-α-$[X_2W_{15}O_{56}]^{12-}$ ($X = P^V$, As^V) fragments and four transition-metal centers constitute a well-known class of compounds.[11] The first example of this type, $[Co_4(H_2O)_2(PW_9O_{34})_2]^{10-}$, was reported by Weakley et al.[11a] Later, Finke and Droege reported on an analogous structural type based on two lacunary Wells−Dawson ions, $[M_4(H_2O)_2(P_2W_{15}O_{56})_2]^{16-}$ ($M = Co^{2+}$, Cu^{2+}, Zn^{2+}).[11c] Evans et al. were the first to report on a As(V) derivative of the Keggin type, $[Zn_4(H_2O)_2(AsW_9O_{34})_2]^{10-}$.[11d] Recently, Bi et al. described the first arsenic(V) analogues of the Wells−Dawson type, $([M_4(H_2O)_2(As_2W_{15}O_{56})_2]^{16-}$ ($M = Mn^{2+}$, Co^{2+}, Ni^{2+}, Cu^{2+}, Zn^{2+}, Cd^{2+}), and the same authors extended the Keggin series by several compounds, $[M_4(H_2O)_2(AsW_9O_{34})_2]^{10-}$ ($M = Mn^{2+}$, Co^{2+}, Ni^{2+}, Cu^{2+}, Zn^{2+}, Cd^{2+}, Fe^{2+}).[11p,q] Kortz et al. reported on the first examples of sandwich-type silicotungstates, $[M_4(H_2O)_2(SiW_9O_{34})_2]^{12-}$ ($M = Mn^{2+}$, Cu^{2+}, Zn^{2+}).[11r] These polyanions were synthesized from the dilacunary, metastable precursor [γ-$SiW_{10}O_{36}]^{8-}$.

Recently, Hill and co-workers described the first examples of sandwich-type species with less than four transition metals, $[Fe_2(NaOH_2)_2(P_2W_{15}O_{56})_2]^{16-}$ and $[Fe_2(FeOH_2)(NaOH_2)(P_2W_{15}O_{56})_2]^{14-}$.[12,13] The di-iron-substituted species reacts with Cu^{2+} or Co^{2+} ions in aqueous solution, leading to a trisubstituted mixed-metal sandwich-type polyanion.[14] The di- and trisubstituted cobalt(II) analogues of this polyanion are also known.[15] Very recently, Kortz et al. reported on the first example of a trisubstituted sandwich-type polyoxoanion based on the *B*-α-$[PW_9O_{34}]^{9-}$ Keggin fragment, $[Ni_3Na(H_2O)_2(PW_9O_{34})_2]^{11-}$.[16]

The number of germanium-containing polyoxoanions is very small and most of the published work is based on the Keggin-type germanododecamolybdate, $[GeMo_{12}O_{40}]^{4-}$, and the analogous germanotungstate, $[GeW_{12}O_{40}]^{4-}$.[17] In 1977 Hervé and Tézé reported on different isomers of the first

(5) *Polyoxometalates: From Platonic Solids to Anti-Retroviral Activity*; Pope, M. T., Müller, A., Eds.; Kluwer: Dordrecht, The Netherlands, 1994.

(6) *Chemical Reviews*, Thematic Issue on Polyoxometalates; Hill, C. L., Ed.; American Chemical Society: Washington, DC, 1998.

(7) *Polyoxometalate Chemistry: From Topology via Self-Assembly to Applications*; Pope, M. T., Müller, A., Eds.; Kluwer: Dordrecht, The Netherlands, 2001.

(8) *Polyoxometalate Chemistry for Nano-Composite Design*; Yamase, T., Pope, M. T., Eds.; Kluwer: Dordrecht, The Netherlands, 2002.

(9) Gatteschi, D. *Adv. Mater.* **1994**, *6*, 635.

(10) *Magnetic Molecular Materials*; Gatteschi, D., Kahn, O., Miller, J. S., Palacio, F., Eds.; Kluwer: Dordrecht, The Netherlands, 1991.

(11) (a) Weakley, T. J. R.; Evans, H. T. jun.; Showell, J. S.; Tourné, G. F.; Tourné, C. M. *J. Chem. Soc., Chem. Commun.* **1973**, 139. (b) Finke, R. G.; Droege, M.; Hutchinson, J. R.; Gansow, O. *J. Am. Chem. Soc.* **1981**, *103*, 1587. (c) Finke, R. G.; Droege, M. W. *Inorg. Chem.* **1983**, *22*, 1006. (d) Evans, H. T.; Tourné, C. M.; Tourné, G. F.; Weakley, T. J. R. *J. Chem. Soc., Dalton Trans.* **1986**, 2699. (e) Finke, R. G.; Droege, M. W.; Domaille, P. J. *Inorg. Chem.* **1987**, *26*, 3886. (f) Wasfi, S. H.; Rheingold, A. L.; Kokoszka, G. F.; Goldstein, A. S. *Inorg. Chem.* **1987**, *26*, 2934. (g) Weakley, T. J. R.; Finke, R. G. *Inorg. Chem.* **1990**, *29*, 1235. (h) Gómez-García, C. J.; Coronado, E.; Borrás-Almenar, J. J. *Inorg. Chem.* **1992**, *31*, 1667. (i) Casañ-Pastor, N.; Bas-Serra, J.; Coronado, E.; Pourroy, G.; Baker, L. C. W. *J. Am. Chem. Soc.* **1992**, *114*, 10380. (j) Gómez-García, C. J.; Coronado, E.; Gómez-Romero, P.; Casañ-Pastor, N. *Inorg. Chem.* **1993**, *32*, 3378. (k) Gómez-García, C. J.; Borrás-Almenar, J. J.; Coronado, E.; Ouahab, L. *Inorg. Chem.* **1994**, *33*, 4016. (l) Zhang, X.-Y.; Jameson, G. B.; O'Connor, C. J.; Pope, M. T. *Polyhedron* **1996**, *15*, 917. (m) Zhang, X.; Chen, Q.; Duncan, D. C.; Campana, C.; Hill, C. L. *Inorg. Chem.* **1997**, *36*, 4208. (n) Zhang, X.; Chen, Q.; Duncan, D. C.; Lachicotte, R. J.; Hill, C. L. *Inorg. Chem.* **1997**, *36*, 4381. (o) Clemente-Juan, J. M.; Coronado, E.; Galán-Mascarós, J. R.; Gómez-García, C. J. *Inorg. Chem.* **1999**, *38*, 55. (p) Bi, L.-H.; Wang, E.-B.; Peng, J.; Huang, R.-D.; Xu, L.; Hu, C.-W. *Inorg. Chem.* **2000**, *39*, 671. (q) Bi, L.-H.; Huang, R.-D.; Peng, J.; Wang, E.-B.; Wang, Y.-H.; Hu, C.-W. *J. Chem. Soc., Dalton Trans.* **2001**, 121. (r) Kortz, U.; Isber, S.; Dickman, M. H.; Ravot, D. *Inorg. Chem.* **2000**, *39*, 2915. (s) Limanski, E. M.; Piepenbrink, M.; Droste, E.; Burgemeister, K.; Krebs, B. *J. Clust. Sci.* **2002**, *13*, 369. (t) Rosu, C.; Crans, D. C.; Weakley, T. J. R. *Polyhedron* **2002**, *21*, 959.

(12) (a) Zhang, X.; Anderson, T. M.; Chen, Q.; Hill, C. L. *Inorg. Chem.* **2001**, *40*, 418. (b) Zhang, X.; Hill, C. L. *Chem. Ind.* **1998**, *75*, 519.

(13) Anderson, T. M.; Zhang, X.; Hardcastle, K. I.; Hill, C. L. *Inorg. Chem.* **2002**, *41*, 2477.

(14) Anderson, T. M.; Hardcastle, K. I.; Okun, N.; Hill, C. L. *Inorg. Chem.* **2001**, *40*, 6418.

(15) Ruhlmann, L.; Canny, J.; Contant, R.; Thouvenot, R. *Inorg. Chem.* **2002**, *41*, 3811.

(16) Kortz, U.; Mbomekalle, I. M.; Keita, B.; Nadjo, L. *Inorg. Chem.* **2002**, *41*, 6412.

monolacunary germanotungstate, $[GeW_{11}O_{39}]^{8-}$.[18] In 1993 Liu et al. reported on the trivanadium-substituted $[GeW_9V_3O_{40}]^{7-}$.[19] In 1994 Qu et al. reported on a series of trisubstituted, monomeric germanotungstates, *A*-α-$[M_3(H_2O)_3GeW_9O_{37}]^{n-}$ ($n = 7$, M = Cr^{3+}; $n = 10$, M = Mn^{2+}, Co^{2+}, Ni^{2+}, Cu^{2+}).[20] In the following year Meng and Liu and others reported on the analogous monomeric polyanion $[M_3(H_2O)_3GeW_9O_{37}]^{7-}$ (M = Al^{3+}, Ga^{3+}, In^{3+}) and the dimeric species α-$[Ga_6(H_2O)_3(GeW_9O_{37})_2]^{14-}$.[21] In the same year Meng and Liu and others reported on the analogous titanium-substituted species *A*-*β*-$[Ti_6O_3(GeW_9O_{37})_2]^{14-}$.[22] Recently, Craciun and David reported on the triuranium(IV)-substituted germanotungstate $[(UO)_3(GeW_9O_{34})_2]^{14-}$.[23] However, the proposed formulas and structures of all transition-metal-substituted species mentioned above remain to be confirmed by X-ray diffraction.

Here, we report for the first time on structurally characterized transition-metal-substituted germanotungstates of the sandwich type.

Experimental Section

Synthesis. All reagents were used as purchased without further purification.

$Na_{12}[Mn_4(H_2O)_2(GeW_9O_{34})_2]\cdot 38H_2O$ (Na_{12}-1). The following reagents were dissolved in 40 mL of a 0.5 M sodium acetate buffer (pH 4.8) with stirring in this order: 0.388 g (1.96 mmol) of $MnCl_2\cdot 4H_2O$, 0.0928 g (0.888 mmol) of GeO_2, and 2.64 g (8.00 mmol) of $Na_2WO_4\cdot 2H_2O$. This solution was heated to 90 °C for 1 h and then cooled to room temperature. Slow evaporation of this solution resulted in single crystals suitable for X-ray crystallography (yield: 1.8 g, 69%). IR: 942 (s), 875 (s), 767 (vs), 709 (s), 510 (w), 463 (w), 444 (w) cm^{-1}. Anal. Calcd (Found) for $Na_{12}[Mn_4(H_2O)_2(GeW_9O_{34})_2]$: Na 5.4 (5.2), Mn 4.3 (4.3), Ge 2.9 (2.7), W 65.2 (63.6). The sample for elemental analysis was dried in an oven at 120 °C overnight.

$Na_{11}Cs_2[Cu_4(H_2O)_2(GeW_9O_{34})_2]Cl\cdot 31H_2O$ (Na_{11}Cs-2). The synthetic procedure above was followed using 0.334 g (1.96 mmol) of $CuCl_2\cdot 2H_2O$ instead of $MnCl_2\cdot 4H_2O$. Single crystals suitable for X-ray crystallography were obtained by layering of the above solution with a dilute CsCl solution and slow evaporation (yield: 1.8 g, 71%). IR: 941 (s), 890 (s), 846 (w), 775 (vs), 734 (s), 718 (s), 509 (w), 469 (w), 438 (w) cm^{-1}. Anal. Calcd (Found) for $Na_{11}Cs_2[Cu_4(H_2O)_2(GeW_9O_{34})_2]Cl\cdot 31H_2O$: Na 4.3 (4.4), Cs 4.5 (4.3), Cu 4.3 (4.5), Ge 2.4 (2.4), W 55.7 (56.4).

$Na_{12}[Zn_4(H_2O)_2(GeW_9O_{34})_2]\cdot 32H_2O$ (Na_{12}-3). The procedure above was followed using 0.267 g (1.96 mmol) of $ZnCl_2$. Slow evaporation of the solution resulted in single crystals suitable for X-ray crystallography (yield: 1.9 g, 75%). IR: 946 (s), 888 (s), 837 (w), 772 (vs), 705 (s), 511 (w), 454 (w) cm^{-1}. Anal. Calcd (Found) for $Na_{12}[Zn_4(H_2O)_2(GeW_9O_{34})_2]\cdot 32H_2O$: Na 4.9 (5.2), Zn 4.6 (4.9), Ge 2.6 (2.9), W 58.1 (59.3). Tungsten-183 NMR (D_2O, 293 K) for $Na_{12}[Zn_4(H_2O)_2(GeW_9O_{34})_2]\cdot 32H_2O$: δ −85.5 ppm (singlet, 2W), −103.9 ppm (singlet, 4W), −107.8 ppm (singlet, 4W), −137.2 ppm (singlet, 4W), −140.1 ppm (singlet, 4W).

$Na_{12}[Cd_4(H_2O)_2(GeW_9O_{34})_2]\cdot 32.2H_2O$ (Na_{12}-4). The procedure above was followed using 0.359 g (1.96 mmol) of $CdCl_2$. Single-crystalline material was obtained by slow evaporation of the above solution (yield: 1.8 g, 70%). IR: 937 (s), 881 (s), 837 (w), 760 (vs), 708 (s), 511 (w), 460 (w), 443 (w) cm^{-1}. Anal. Calcd (Found) for $Na_{12}[Cd_4(H_2O)_2(GeW_9O_{34})_2]\cdot 32.2H_2O$: Na 4.7 (5.1), Cd 7.6 (8.1), Ge 2.5 (2.4), W 56.2 (57.1). Tungsten-183 NMR (D_2O, 313 K) for $Na_{12}[Cd_4(H_2O)_2(GeW_9O_{34})_2]\cdot 32.2H_2O$: δ −80.5 ppm (singlet, 2W), −100.1 ppm (singlet, 4W), −104.2 ppm (singlet, 4W), −118.6 ppm (singlet, 4W), −124.4 ppm (singlet, 4W).

All elemental analyses were performed by Kanti Labs Ltd. in Mississauga, Canada. The IR spectra were recorded on a Nicolet Avatar FTIR spectrophotometer in a KBr pellet. The ^{183}W-NMR spectra were recorded on a JEOL Eclipse 400+ instrument at 16.67 MHz using D_2O as a solvent in 10-mm tubes. Solid samples of **Na_{12}-3** and **Na_{12}-4** were dissolved in D_2O upon addition of solid $LiClO_4$ and heating. The measurement of **Na_{12}-4** was done at 40 °C to avoid precipitation of the polyanion salt.

Magnetic measurements of **Na_{12}-1** and **Na_{11}Cs-2** were carried out using a Quantum Design MPMS-XL SQUID magnetometer. Data for polycrystalline samples of **Na_{12}-1** and **Na_{11}Cs-2** were collected over the temperature range 1.8−200 K up to 7 T. Polycrystalline powder EPR spectra of **Na_{12}-1** and **Na_{11}Cs-2** were recorded using a Bruker Elexsys-500 spectrometer at X-band (∼9.5 GHz) in the temperature range 4−300 K. High-frequency EPR experiments were conducted on a custom-built variable frequency EPR spectrometer at the National High Magnetic Field Laboratory in Tallahassee.[24] All simulations were obtained with the Bruker XSophe program. Experimental parameters were used with the appropriate spin Hamiltonian to generate the simulated spectrum.

X-ray Crystallography. Crystals of compounds **Na_{11}Cs-2**, **Na_{12}-3**, and **Na_{12}-4** were mounted on a glass fiber for indexing and intensity data collection at 173 K on a Siemens SMART CCD single-crystal diffractometer using Mo Kα radiation ($\lambda = 0.71073$ Å). Direct methods were used to solve the structures and to locate the heavy atoms (SHELXS86). Then the remaining atoms were found from successive difference maps (SHELXL93).

A crystal of compound **Na_{12}-1** was mounted on a glass fiber for indexing and intensity data collection at 200 K on a Bruker D8 SMART APEX CCD single-crystal diffractometer using Mo Kα radiation ($\lambda = 0.71073$ Å). Direct methods were used to solve the structure and to locate the heavy atoms (SHELXS97). Then the remaining atoms were found from successive difference maps (SHELXL97).

Routine Lorentz and polarization corrections were applied and an absorption correction was performed using the SADABS program.[25] Crystallographic data are summarized in Table 1.

(17) (a) Katano, H.; Osakai, T.; Himeno, S.; Saito, A. *Electrochim. Acta* **1995**, *40*, 2935. (b) Wilde, W.; Baeker, C.; Lunk, H. J. *Z. Chem.* **1989**, *29*, 346. (c) Dorokhova, E. N.; Kazanskii, L. P.; Prokhorova, G. V. *Zh. Neorg. Khim.* **1985**, *30*, 2795. (d) Biquard, M.; Souchay, P. *Ann. Chim. Paris* **1975**, *10*, 163. (e) Biquard, M. *C. R. Acad. Sci. Ser. C* **1975**, *281*, 309. (f) Leyrie, M.; Herve, G. *C. R. Acad. Sci. Ser. C* **1973**, *276*, 911. (g) Biquard, M.; Lamache, M. *Bull. Soc. Chim. France* **1971**, *1*, 32.

(18) Hervé, G.; Tézé, A. *Inorg. Chem.* **1977**, *16*, 2115.

(19) (a) Liu, J. F.; Zhao, B. L.; Rong, C. Y.; Pope, M. T. *Acta Chim. Sin.* **1993**, *51*, 368. (b) Liu, J. F.; Zhen, Y. G.; So, H. S. *Synth. React. Inorg. Met.-Org. Chem.* **1998**, *28*, 863.

(20) Qu, L. Y.; Sun, Y. J.; Chen, Y. G.; Yu, M.; Peng, J. *Synth. React. Inorg. Met.-Org. Chem.* **1994**, *24*, 1339.

(21) (a) Meng, L.; Liu, J. F. *Chin. J. Chem.* **1995**, *13*, 334. (b) Meng, L.; Zhan, X. P.; Wang, M.; Liu, J. F. *Polyhedron* **2001**, *20*, 881.

(22) (a) Meng, L.; Liu, J. F. *Chin. Chem. Lett.* **1995**, *6*, 265. (b) Liu, J. F.; Wang, X. H.; Ma, J. F.; Meng, L.; Yang, Q. H. *Chem. J. Chin. U.* **1999**, *20*, 696. (c) Liu, J. F.; Wang, X. H.; Ma, J. F.; Meng, L. *Acta Chim. Sin.* **1999**, *57*, 769.

(23) Craciun, C.; David, L. *J. Alloys Compd.* **2001**, *323*, 743.

(24) (a) Hassan, A. K.; Pardi, L. A.; Krzystek, J.; Sienkiewicz, A.; Goy, P.; Rohrer, M.; Brunel, L. C. *J. Magn. Reson.* **2000**, *142*, 300. (b) Cage, B.; Hassan, A. K.; Pardi, L.; Krzystek, J.; Brunel, L. C.; Dalal, N. S. *J. Magn. Reson.* **1997**, *124*, 495.

(25) Sheldrick, G. M. *SADABS*; University of Göttingen: Göttingen, Germany, 1996.

Table 1. Crystal Data and Structure Refinement for $Na_{12}[Mn_4(H_2O)_2(GeW_9O_{34})_2]\cdot 38H_2O$ (**Na_{12}-1**), $Na_{11}Cs_2[Cu_4(H_2O)_2(GeW_9O_{34})_2]Cl\cdot 31H_2O$ (**Na_{11}Cs-2**), $Na_{12}[Zn_4(H_2O)_2(GeW_9O_{34})_2]\cdot 32H_2O$ (**Na_{12}-3**), and $Na_{12}[Cd_4(H_2O)_2(GeW_9O_{34})_2]\cdot 32.2H_2O$ (**Na_{12}-4**)

	Na_{12}-1	**Na_{11}Cs-2**	**Na_{12}-3**	**Na_{12}-4**
emp formula	$Ge_2H_{80}Mn_4Na_{12}O_{108}W_{18}$	$ClCs_2Cu_4Ge_2H_{66}Na_{11}O_{101}W_{18}$	$Ge_2H_{68}Na_{12}O_{102}W_{18}Zn_4$	$Cd_4Ge_2Na_{12}O_{102.2}W_{18}$
fw	5758.9	5945.5	5692.6	5815.2
space group (No.)	$P2_1/n$ (14)	$P\bar{1}$ (2)	$P\bar{1}$ (2)	$P\bar{1}$ (2)
a (Å)	13.0419(8)	12.2338(17)	11.589(3)	11.6923(17)
b (Å)	17.8422(10)	12.3833(17)	12.811(3)	12.8464(18)
c (Å)	21.1626(12)	15.449(2)	17.221(4)	17.616(2)
α (deg)		100.041(2)	97.828(6)	98.149(3)
β (deg)	93.3120(10)	97.034(2)	106.169(6)	105.677(3)
γ (deg)		101.153(2)	112.113(5)	112.233(2)
vol (Å^3)	4916.2(5)	2231.3(5)	2189.9(9)	2268.0(6)
Z	2	1	1	1
temp (°C)	−73	−100	−100	−100
wavelength (Å)	0.710 73	0.710 73	0.710 73	0.710 73
d_{calcd} (Mg m^{-3})	3.82	4.36	4.26	4.26
abs coeff. (mm^{-1})	22.229	25.696	25.468	24.470
R [$I > 2\sigma(I)$][a]	0.077	0.041	0.045	0.059
R_w (all data)[b]	0.138	0.101	0.099	0.143

[a] $R = \sum||F_o| - |F_c||/\sum|F_o|$. [b] $R_w = [\sum w(F_o^2 - F_c^2)^2/\sum w(F_o^2)^2]^{1/2}$.

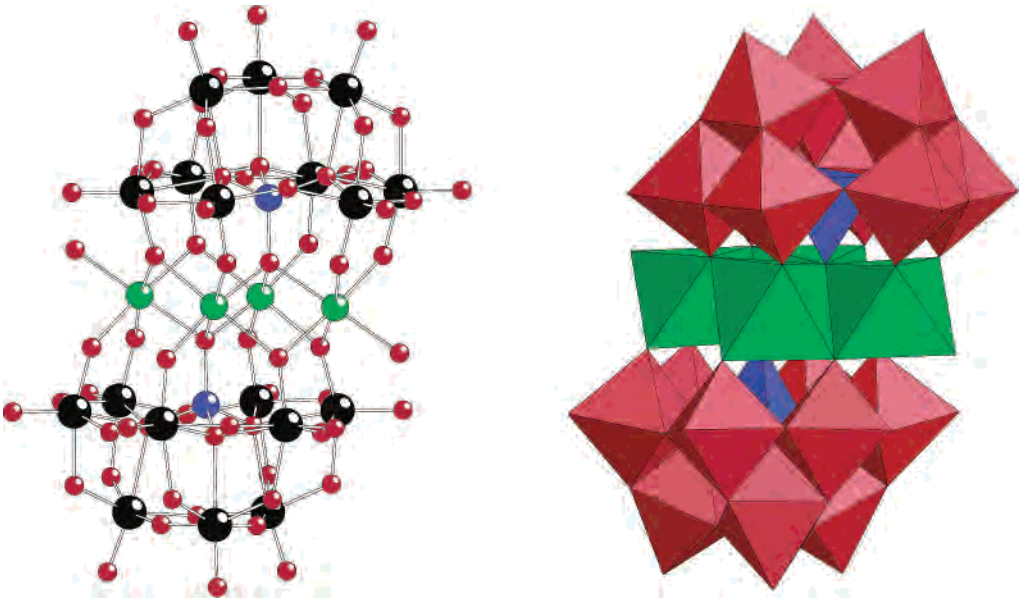

Figure 1. Ball and stick (left) and polyhedral (right) representations of $[Mn_4(H_2O)_2(GeW_9O_{34})_2]^{12-}$ (**1**). The color code is as follows: manganese (green), tungsten (black), germanium (blue), and oxygen (red). This figure is also representative of the structures of the remaining three polyanions $[Cu_4(H_2O)_2(GeW_9O_{34})_2]^{12-}$ (**2**), $[Zn_4(H_2O)_2(GeW_9O_{34})_2]^{12-}$ (**3**), and $[Cd_4(H_2O)_2(GeW_9O_{34})_2]^{12-}$ (**4**).

Results and Discussion

Synthesis and Structure. The four novel dimeric germanotungstates $[Mn_4(H_2O)_2(GeW_9O_{34})_2]^{12-}$ (**1**), $[Cu_4(H_2O)_2(GeW_9O_{34})_2]^{12-}$ (**2**), $[Zn_4(H_2O)_2(GeW_9O_{34})_2]^{12-}$ (**3**), and $[Cd_4(H_2O)_2(GeW_9O_{34})_2]^{12-}$ (**4**) consist of two lacunary *B*-α-$[GeW_9O_{34}]^{10-}$ Keggin moieties linked via a rhomblike M_4O_{16} (M = Mn, Cu, Zn, Cd) group leading to a sandwich-type structure (see Figure 1). This structural type had first been described in 1973 by Weakley et al. for $[Co_4(H_2O)_2(PW_9O_{34})_2]^{10-}$.[11a] By now this Keggin-based architecture is known for most first-row transition metals (including mixed metal) and it has also been possible to substitute the tetrahedral phosphorus(V) heteroatom by arsenic(V), silicon(IV), iron(III), and copper(II).[11] Therefore, this structural type represents one of the largest transition-metal-substituted polyoxoanion families. However, the title polyanions represent the first example of transition-metal-substituted germanotungstates of this sandwich type.

The synthesis of $[M_4(H_2O)_2(GeW_9O_{34})_2]^{12-}$ (M = Mn^{2+}, Cu^{2+}, Zn^{2+}, Cd^{2+}) is based on reaction of the three components GeO_2, Na_2WO_4, and a source of the respective transition-metal ions manganese(II), copper(II), zinc(II), and cadmium(II) in an aqueous, acidic medium. The isolated yields for **1**−**4** are in the range of 75−80%, which indicates that formation of the (*B*-α-GeW_9O_{34}) fragment in a heated aqueous acidic medium is strongly favored. Most likely synthesis of this trilacunary building block is further facilitated by the presence of transition-metal ions and the formation of the dimeric polyanions **1**−**4**. We were able to determine the solid-state structures of **1**−**4** by single-crystal X-ray diffraction and we discovered that the structures of the zinc and cadmium derivatives **Na_{12}-3** and **Na_{12}-4**, respectively, are isomorphous. The tungsten-oxo bond dis-

Table 2. Selected Bond Distances (Å) and Angles (deg) for $[Mn_4(H_2O)_2(GeW_9O_{34})_2]^{12-}$ (**1**), $[Cu_4(H_2O)_2(GeW_9O_{34})_2]^{12-}$ (**2**), $[Zn_4(H_2O)_2(GeW_9O_{34})_2]^{12-}$ (**3**), and $[Cd_4(H_2O)_2(GeW_9O_{34})_2]^{12-}$ (**4**)

	1	**2**	**3**	**4**
M_{int}−O(Ge)	2.176(12)	1.973−1.986(8)	2.110−2.114(9)	2.291−2.313(12)
M_{int}−O(W)	2.079−2.097(12)	1.931(8)	2.045−2.052(10)	2.213−2.242(13)
M_{int}−O(W,M)	2.194−2.224(13)	2.406−2.427(8)	2.155−2.176(9)	2.290−2.294(13)
M_{ext}−O(Ge)	2.195(12)	2.364(7)	2.104(9)	2.300(12)
M_{ext}−OH_2	2.277(16)	2.346(8)	2.098(9)	2.260(14)
M_{ext}−O(W)	2.125−2.141(14)	1.969−1.974(8)	2.050−2.116(10)	2.229−2.281(13)
M_{ext}−O(W,M)	2.177−2.185(12)	1.966−1.988(8)	2.108−2.133(10)	2.280−2.286(13)
Ge···Ge	5.880(2)	5.732(2)	5.817(2)	6.073(2)
M_{int}···M_{int}'	3.318(2)	3.069(2)	3.208(2)	3.478(2)
M_{int}···M_{ext}	3.254, 3.270(2)	3.174, 3.176(2)	3.144, 3.181(2)	3.357, 3.404(2)
M_{ext}···M_{ext}'	5.617(2)	5.559(2)	5.451(2)	5.798(2)
M_{ext}−O(Ge)−M_{int}	96.2, 96.9(5)	93.3, 93.7(3)	96.5, 97.9(4)	93.4, 95.7(4)
M_{int}−O(Ge)−M_{int}'	99.4(5)	101.7(3)	98.8(4)	98.1(4)
M_{ext}−O−M_{int}	95.4, 96.6(5)	91.9, 92.1(3)	94.3, 95.9(4)	94.3, 96.2(5)

tances and angles of all four structures are within the usual ranges. However, there are subtle structural differences among polyanions **1**−**4**, which are centered around the rhomblike M_4O_{16} (M = Mn, Cu, Zn, Cd) group (see Figure 2). It is not unexpected that the M−O bond lengths within the octahedral coordination spheres of Mn^{2+}, Cu^{2+}, Zn^{2+}, and Cd^{2+} are different (see Table 2). This leads to different separations of the two (*B*-α-GeW_9O_{34}) fragments within each polyanion, which can be expressed by the distance between the two germanium heteroatoms within each polyanion: **1**: 5.880(2), **2**: 5.732(2), **3**: 5.817(2), and **4**: 6.073(2) Å. As expected, the Ge···Ge distance is largest for the cadmium-derivative **4**, which reflects the larger size of the Cd^{2+} ion compared with that of the 3d metal ions Mn^{2+}, Cu^{2+}, and Zn^{2+}. It is also not unexpected that in **2** the Ge···Ge distance is smallest, which indicates the Jahn−Teller distortion of the CuO_6 octahedra. For the remaining two polyoxoanions **1** and **3** we observe the expected regular coordination environments for Mn^{2+} (d^5, high spin) and Zn^{2+} (d^{10}). Interestingly, the Ge···Ge distance in **1** and **3** is in complete agreement with the size difference of the Mn^{2+} and Zn^{2+} ions.

Bond-valence sum calculations for **1**−**4** indicated that the terminal oxygen atoms associated with two of the four transition-metal ions in the central plane are the only protonation sites of the polyanions.[26] In polyoxoanion chemistry it is highly unusual that all sodium cations can be identified because of commonly observed disorder. However, we were able to account for all required countercations by X-ray diffraction for **Na_{12}-1**, **Na_{11}Cs-2**, **Na_{12}-3**, and **Na_{12}-4**. This indicates very good quality single crystals and most likely very stable solid-state lattices. The structure of **Na_{11}Cs-2** is a mixed sodium−cesium salt and interestingly 1 equiv of CsCl cocrystallized with polyoxoanion **2**. The elemental composition of all four structures based on X-ray diffraction is fully supported by the results of elemental analysis.

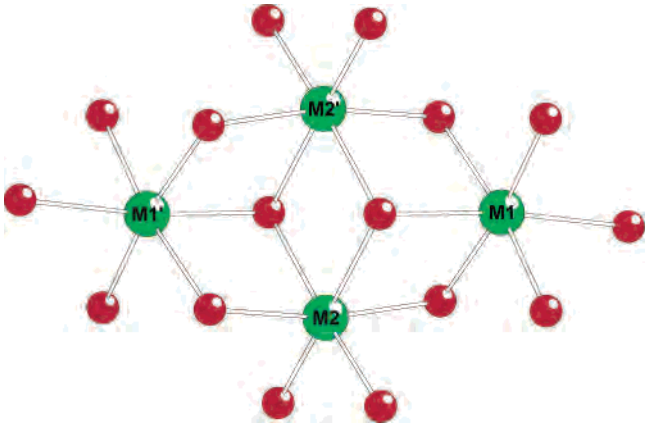

Figure 2. Ball and stick representation of the central M_4O_{16} (M = Mn^{2+}, Cu^{2+}, Zn^{2+}, Cd^{2+}) fragment of polyoxoanions **1**−**4**.

The dimeric polyanions **1**−**3** are very closely related to the silicon-containing analogues $[M_4(H_2O)_2(SiW_9O_{34})_2]^{12-}$ (M = Mn^{2+}, Cu^{2+}, Zn^{2+}), which are structurally equivalent and also have the same charge.[11r] However, the synthetic procedures for the silicotungstates and the germanotungstates are very different. Synthesis of the former was based on reaction of transition-metal ions with the divacant, metastable γ-decatungstosilicate, [γ-$SiW_{10}O_{36}]^{8-}$. Therefore, the reaction mechanism must include metal insertion, isomerization ([γ-$SiW_{10}O_{36}]^{8-}$ → *B*-α-$[SiW_9O_{34}]^{10-}$), dimerization, and loss of tungsten. Compared to this, the synthesis of **1**−**4** appears more rational and direct because it involves a one-step reaction using a source of all required elements (Ge, W, and Mn, Cu, Zn, or Cd) in appropriate molar ratios. No heteropolyanionic precursor is required for the synthesis of **1**−**4**, but we were interested if the same compounds could also be synthesized from the known precursor *A*-$[GeW_9O_{34}]^{10-}$. Therefore, we prepared this trilacunary polyanion according to the procedure of Hervé and Tézé[27] and reacted it with Cu^{2+}, Mn^{2+}, Zn^{2+}, and Cd^{2+} ions using the same conditions as for the syntheses of **1**−**4**. On the basis of IR, we are certain that indeed we obtained polyanions **1**−**4**, which means that the isomerization *A*-$[GeW_9O_{34}]^{10-}$ → *B*-$[GeW_9O_{34}]^{10-}$ has occurred during the course of the reaction in an aqueous, acidic medium upon heating.

To learn more about the solution properties of **1**−**4**, we decided to investigate them by ^{183}W-NMR. This technique is especially adapted for the diamagnetic polyoxoanions **3** and **4**. The room-temperature ^{183}W-NMR spectrum of **3** exhibits five peaks at −85.5, −103.9, −107.8, −137.2, and −140.1 ppm with intensity ratios 1:2:2:2:2 (see Figure 3). For **4** we also obtained a spectrum with five peaks at −80.5,

(26) Brown, I. D.; Altermatt, D. *Acta Crystallogr.* **1985**, *B41*, 244.
(27) Hervé G.; Tézé, A. *Inorg. Chem.* **1977**, *16*, 2115.

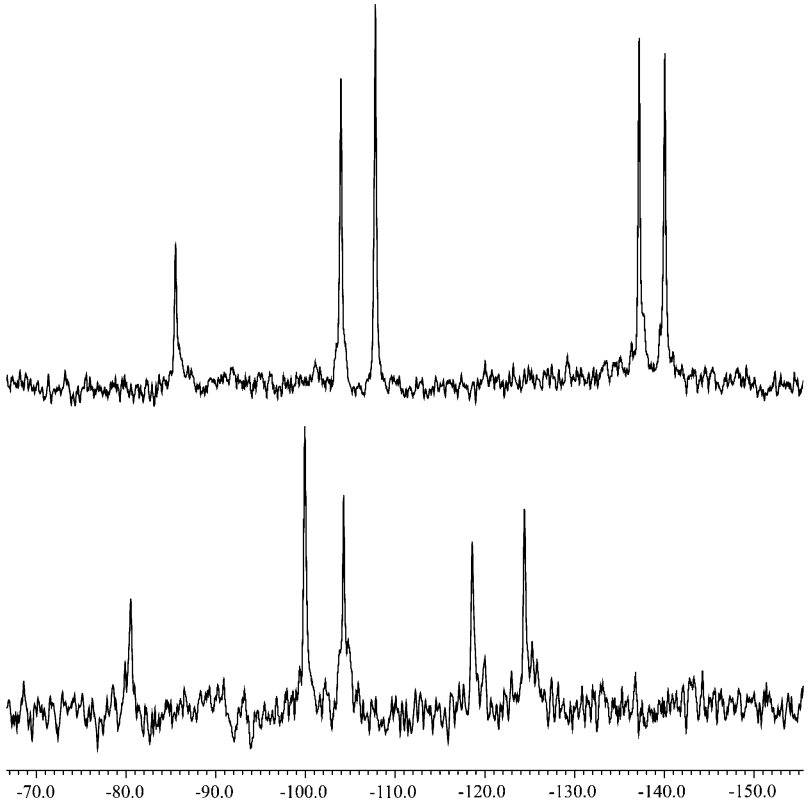

Figure 3. Tungsten-183 NMR spectra of $Na_{12}[Zn_4(H_2O)_2(GeW_9O_{34})_2]\cdot 32H_2O$ (**Na_{12}-3**) at 293 K, top, and $Na_{12}[Cd_4(H_2O)_2(GeW_9O_{34})_2]\cdot 32.2H_2O$ (**Na_{12}-4**) at 313 K, bottom.

−100.1, −104.2, −118.6, and −124.4 ppm and the expected intensity ratios 1:2:2:2:2 (see Figure 3). If the dimeric, sandwich-type structures of **3** and **4** with C_{2h} symmetry are preserved in solution, then exactly this peak pattern is expected. We can conclude that the solid-state structures of both polyanions **3** and **4** are preserved in solution after redissolution.

Magnetic Studies. The temperature dependence of $\chi_m T$ of **Na_{12}-1** (see Figure 4a) shows a very small decrease between 250 and 100 K from ∼19 to ∼18 emu K/mol G and then an exponential decrease down to 1.8 K. The magnetization of **Na_{12}-1** (see Figure 4b) increases steeply up to about 3 T and then increases linearly without reaching saturation up to 7 T.

Figure 4c shows the temperature dependence of $\chi_m T$ of **Na_{11}Cs-2** over 1.8−200 K. $\chi_m T$ decreases exponentially up to 50 K, reaches a saturation value of ∼0.94 emu K/mol G between 50 and 10 K, and then decreases until 1.8 K due to intermolecular interactions. The magnetization of **Na_{11}Cs-2** reaches saturation (∼2 μ_B) at 6 T (see Figure 4d).

The individual metal ions of each tetrameric M_4O_{16} (M = Mn^{2+}, Cu^{2+}) unit interact with each other via M−O−M bridges. To explain the observed magnetic behavior of **Na_{12}-1** and **Na_{11}Cs-2**, the exchange scheme shown in Chart 1 is used.

The corners of the rhombus with the numbers 1, 2, 3, and 4 symbolize the transition-metal ions M1, M2, M1′ and M2′ (M = Mn^{2+}, Cu^{2+}), respectively. The interactions between the metal ions of the M_4O_{16} unit can be described by two

Chart 1

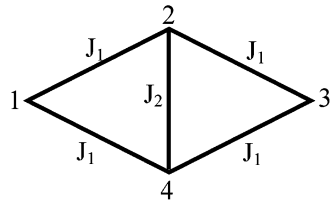

exchange coupling constants J_1 and J_2, where J_1 represents the interactions along the sides of the rhombus while J_2 represents interactions along the short diagonal of the rhombus.

The Heisenberg spin Hamiltonian in the presence of an external magnetic field for this tetrameric cluster is given by eq 1,

$$\mathscr{H} = \beta H\cdot g\cdot(\hat{S}_1 + \hat{S}_2 + \hat{S}_3 + \hat{S}_4) - 2J_1(\hat{S}_1\cdot\hat{S}_2 + \hat{S}_2\cdot\hat{S}_3 + \hat{S}_3\cdot\hat{S}_4 + \hat{S}_1\cdot\hat{S}_4) - 2J_2(\hat{S}_2\cdot\hat{S}_4) \quad (1)$$

where β is the Bohr magneton, H is the external magnetic field, g is the Landé g factor, and $\hat{S}_i$ (i = 1, 2, 3, 4) is the spin operator of the ith metal ion. The eigenvalues of this Hamiltonian are given by eq 2,

$$E(S^T, S_{13}, S_{24}, S, M_{ST}) = M_{ST}g\beta H - J_1[S^T(S^T+1) - S_{13}(S_{13}+1) - S_{24}(S_{24}+1)] - J_2[S_{24}(S_{24}+1) - 2S(S+1)] \quad (2)$$

where $S_{13} = S_1 + S_3$, $S_{24} = S_2 + S_4$, and $S^T = S_{13} + S_{24}$. For **Na_{12}-1**, $S = {}^5/_2$, $0 \le S_{13} \le 5$, $0 \le S_{24} \le 5$, and $|S_{13} - S_{24}|$

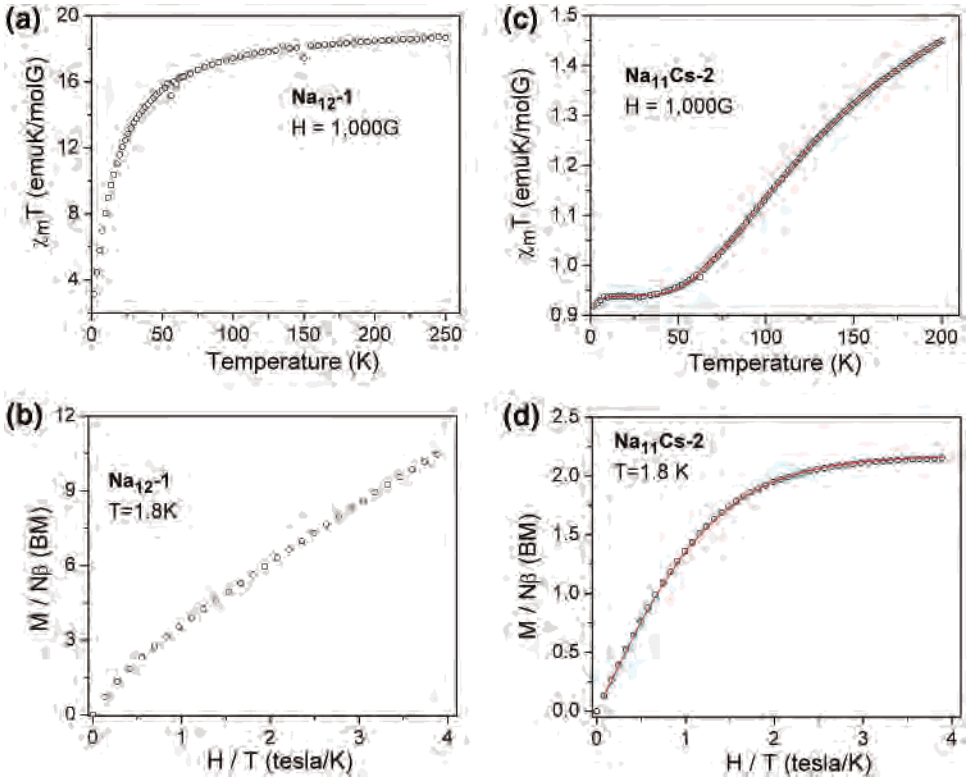

Figure 4. (a) Plot of $\chi_m T$ vs T for $Na_{12}[Mn_4(H_2O)_2(GeW_9O_{34})_2]\cdot 38H_2O$ (**Na_{12}-1**) at 1000 G. (b) Magnetization data of **Na_{12}-1** at 1.8 K. (c) Plot of $\chi_m T$ vs T for $Na_{11}Cs_2[Cu_4(H_2O)_2(GeW_9O_{34})_2]Cl\cdot 31H_2O$ (**Na_{11}Cs-2**) at 1000 G. The solid line represents the theoretical curve (see text). (d) Magnetization data of **Na_{11}Cs-2** at 1.8 K. The solid line represents the theoretical curve (see text).

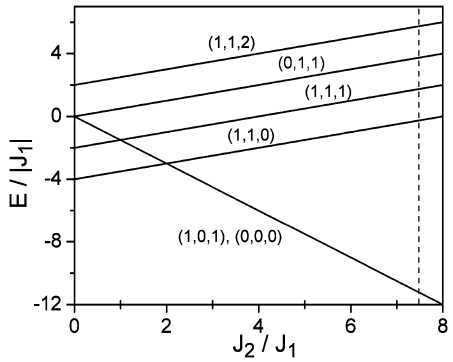

Figure 5. Plot of $E/|J_1|$ as a function of the ratio J_2/J_1 for $Na_{11}Cs_2[Cu_4(H_2O)_2(GeW_9O_{34})_2]Cl\cdot 31H_2O$ (**Na_{11}Cs-2**). The labels indicate (S_{13}, S_{24}, S^T) for each energy level and the vertical dashed line indicates the experimental J_2/J_1 ratio of 7.45.

$\leq S^T \leq S_{13} + S_{24}$ whereas for **Na_{11}Cs-2,** $S = {}^1/_2$, $0 \leq S_{13} \leq 1$, $0 \leq S_{24} \leq 1$, and $|S_{13} - S_{24}| \leq S^T \leq S_{13} + S_{24}$.

The total spin S^T of the M_4O_{16} ($M = Mn^{2+}$, Cu^{2+}) unit is a good quantum number. The dimension of the spin Hamiltonian matrix for Mn_4O_{16} (**Na_{12}-1**) is 1296 × 1296, leading to 6 singlets, 15 triplets, 21 quintets, 24 septets, 24 9-folds, 21 11-folds, 15 13-folds, 10 15-folds, 6 17-folds, 3 19-folds, and 1 21-fold. For Cu_4O_{16} (**Na_{11}Cs-2**) the dimension of the spin Hamiltonian matrix reduces to 16 × 16, leading to 2 singlets, 3 triplets, and 1 quintet.

The magnetization and magnetic susceptibility data analysis of Mn_4O_{16} is currently underway due to the large dimension of the spin Hamiltonian and the results will be published elsewhere.

The magnetic susceptibility data of **Na_{11}Cs-2** was analyzed using eq 3.[28]

$$\chi_m = \left(\frac{Ng^2\beta^2}{3k(T-\theta)}\right)\left(\frac{\sum_n S_n^T(S_n^T+1)(2S_n^T+1)\exp(-E_n/kT)}{\sum_n (2S_n^T+1)\exp(-E_n/kT)}\right) \quad (3)$$

Here, N is the Avogadro number, k the Boltzmann constant, T the temperature in Kelvin, θ the Weiss constant, and E_n the spin exchange energy associated with a spin state S_n^T. A very satisfying description of the experimental data over the whole temperature range (see Figure 4c) is obtained with the following set of parameters: $J_1 = -11$ cm^{-1}, $J_2 = -82$ cm^{-1}, $g_{iso} = 2.24$, and $\theta = -0.035$ cm^{-1}. Figure 5 shows the energy level diagram of $E/|J_1|$ vs J_2/J_1. It can be noticed that, for $J_2 / J_1 \geq 2$, the ground state of the cluster is formed by both triplet and singlet spin states. Thus, in view of our experimental J_2/J_1 ratio (~7.5), the ground state of the Cu_4O_{16} unit is a combination of spin triplet and spin singlet. The intermediate spin ground state results from spin frustration.

In fact, the rhombuslike arrangement can be viewed as being made up of two triangular units sharing a side. Hence, from a thermodynamic point of view a combined spin triplet

(28) (a) Kahn, O. *Molecular Magnetism*; VCH: NewYork, 1993. (b) Kortz, U.; Nellutla, S.; Stowe, A. C.; Dalal, N. S.; van Tol, J.; Bassil, B. S. *Inorg. Chem.* **2004**, *43*, 144.

Table 3. Magnetic Parameters for $Na_{12}[Mn_4(H_2O)_2(GeW_9O_{34})_2]\cdot 38H_2O$ (**Na_{12}-1**) and $Na_{11}Cs_2[Cu_4(H_2O)_2(GeW_9O_{34})_2]Cl\cdot 31H_2O$ (**Na_{11}Cs-2**)

compound	$g_{\|\|}$	$g_\perp$	$A_{\|\|}$ (mT)	$\|D\|$ (mT)	J_1 (cm^{-1})	J_2 (cm^{-1})
Na_{12}-1	$g_{iso} = 1.9949 \pm 0.0008$			20.0 ± 0.1		
Na_{11}Cs-2	2.4303 ± 0.0005	2.0567 ± 0.0005	4.4 ± 0.2	12.1 ± 0.1	-11	-82

and spin singlet ground state is equivalent to that resulting from two independent spin doublets.[11h] Accordingly, the magnetization data at 1.8 K (see Figure 4d) have been fit to eq 4 considering two $S = {}^1/_2$.

$$M = Ng\beta SB_S(\eta) \quad (4)$$

with

$$B_S(\eta) = (1/S)[(S + {}^1/_2)\coth((S + {}^1/_2)\eta) - {}^1/_2\coth(\eta/2)] \quad (5)$$

Here, $B_S(\eta)$ is the Brillouin function, $\eta = g\beta H/kT$, and the variables/constants have their usual meaning. The agreement between theory and experiment is satisfactory when $g_{iso} = 2.17$, in agreement with the EPR results (*vide infra*). This result strongly supports the nature of the ground state deduced by the magnetic susceptibility measurements.

EPR Studies. Variable frequency (9−200 GHz) EPR studies were conducted on a polycrystalline powder sample of **Na_{12}-1** over a temperature range of 4−300 K. Only one broad transition was observed at all frequencies and temperatures investigated. Figure 6 shows the 4 K EPR spectrum at 95 and 188 GHz, respectively. This indicates that the zero-field interaction in **Na_{12}-1** is small and hidden within the experimental line width. The isotropic *g* value for **Na_{12}-1** is 1.9949. Simulations with the Bruker XSophe EPR simulation program yield a satisfactory fit and provide an estimated zero-field splitting ($|D|$) of 12.5−20 mT. Since the possible spin states for **Na_{12}-1** range from 0 to 10, a selection of these states was included in simulating the overall observed EPR spectrum.

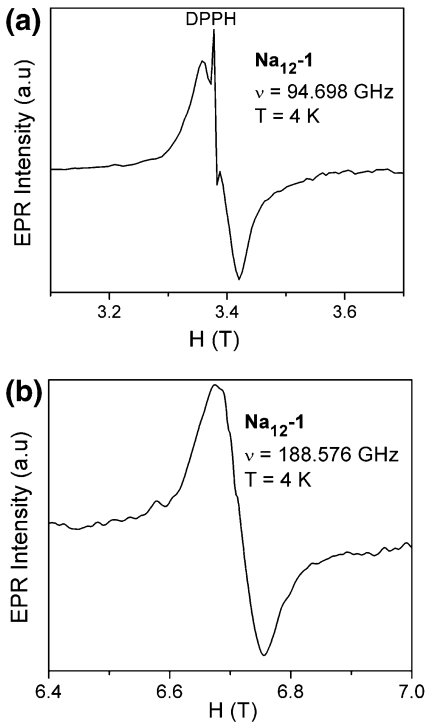

Figure 6. 4 K EPR spectra of $Na_{12}[Mn_4(H_2O)_2(GeW_9O_{34})_2]\cdot 38H_2O$ (**Na_{12}-1**) at (a) 95 GHz and (b) 188 GHz. The sharp central peak in (a) is from the DPPH standard.

The 4 K X-band EPR spectrum of **Na_{11}Cs-2** is shown in Figure 7a where the $S^T = 1$ spin state is observed to be the ground state. The spectral features represent the expected fine structure transitions for a powder spectrum of an $S^T = 1$ spin state. The low field, broader doublet is the parallel feature with a *g* value centered at $g_{||} = 2.4303$. The more intense, sharper lines originate from molecules oriented perpendicular to the applied magnetic field. The splitting between these two lines yields the zero-field splitting parameter ($|D|$) and is 12.1 mT. The *g* value associated with this doublet is $g_\perp = 2.0567$.

With use of the relation $g_{iso} = (2g_\perp + g_{||})/3$, a g_{iso} value of 2.1811 was obtained from the EPR experiments.[29] This value is in good agreement with the magnetization data at 1.8 K. The g_{iso} value from the best fit to the $\chi_m T$ measurements, however, is larger by 3%. This may be due to the small thermal population of the excited states. The EPR and magnetization parameters were obtained at very low temperature where only the ground state should be populated thermally.

A closer look at the parallel transitions reveals hyperfine structure associated with interaction of the unpaired electrons with the ^{63,65}Cu nuclei. There are four Cu^{2+} centers in the molecule which would give a 13 line ($2nI + 1$) pattern should both unpaired electrons be delocalized over all copper atoms. This pattern should be observed on each of the fine structure transitions. However, if the two unpaired electrons are localized on two Cu^{2+} centers, the hyperfine coupling will be reduced significantly and the expected hyperfine splitting pattern would be 7 lines. A 7-line hyperfine splitting pattern is in fact observed (see Figure 7b) with a hyperfine coupling of $A_{||} = 4.4 \pm 0.2$ mT. All the results are summarized in Table 3. No hyperfine structure is observed for the perpendicular lines as the splitting would be smaller. A lower limit of the electron spin-exchange dynamics has been determined to be 4.36×10^{-10} Hz based on the low-temperature X-band EPR results. At higher temperatures, the electron motion is faster and the observed dipolar interactions are averaged out (see Figure 7c).

The W-band EPR spectrum of **Na_{11}Cs-2** has also been analyzed (see Figure 7d). The strong signal again represents the perpendicular transitions of the $S^T = 1$ ground spin state. Resolution of the two transitions is not observed as the zero-field splitting is smaller than the experimental line width. Analysis of the parallel transitions over the temperature range from 2 to 100 K provides information about the sign of the *D* value (see Figure 7d). At 2 K, the low field transition has

(29) Abragam, A.; Bleaney, B. *Electron Paramagnetic Resonance of Transition Ions*; Dover Publications: New York, 1970.

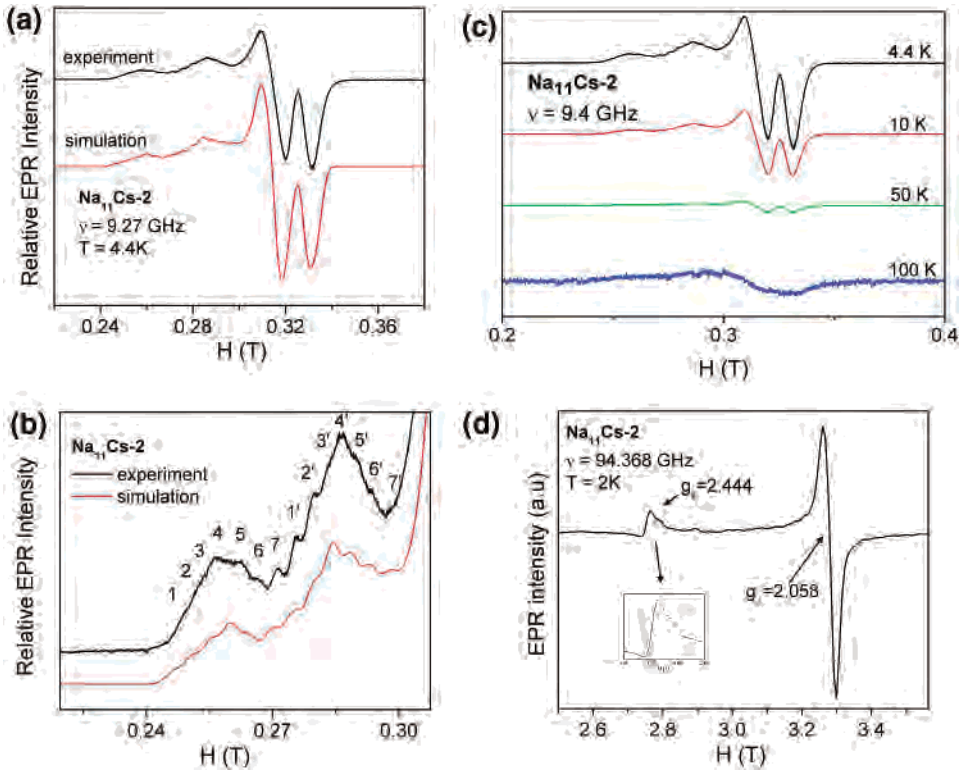

Figure 7. (a) The experimental (black trace) and simulated (red trace) X-band EPR spectra of $Na_{11}Cs_2[Cu_4(H_2O)_2(GeW_9O_{34})_2]Cl\cdot 31H_2O$ (**Na_{11}Cs-2**) at 4 K. The more intense lines are the perpendicular fine structure transitions split by $|D| = 12.0$ mT. Partial resolution of the parallel hyperfine structure is also observed. Experimentally deduced parameters are used in the simulation. (b) A close-up of the hyperfine structure of both parallel fine structure transitions in the X-band spectrum of **Na_{11}Cs-2** at 4 K. The parallel component of the hyperfine splitting is determined to be 4.4 mT. (c) Temperature dependence of the X-band EPR spectrum of **Na_{11}Cs-2**. (d) W-band EPR spectrum of **Na_{11}Cs-2** at 2 K. Full resolution is not observed because the zero-field splitting is smaller than the experimental line width.

the most intensity, indicating a negative D value; that is, $M_{ST} = \pm 1$ is the ground-state energy level.

Conclusions

Four dimeric germanotungstates $[M_4(H_2O)_2(GeW_9O_{34})_2]^{12-}$ ($M = Mn^{2+}$, Cu^{2+}, Zn^{2+}, Cd^{2+}) have been synthesized. Single-crystal X-ray diffraction revealed that the polyanions have a sandwich-type structure and they constitute the first germanotungstate derivatives. This is the first report of polyoxoanions containing the $(B\text{-}\alpha\text{-}GeW_9O_{34})^{10-}$ fragment and **1**−**4** also represent the first examples of structurally characterized germanium-containing heteropolyanions. Synthesis of **1**−**4** was accomplished directly from the composing elements in stoichiometric amounts. This shows once again that a lacunary polyoxoanion precursor is not necessarily needed for the synthesis of substituted polyoxoanions if the reaction conditions are optimized.

Solution ^{183}W-NMR studies on the diamagnetic derivatives **3** and **4** reveal that the solid-state polyanion structure is preserved in solution.

EPR measurements as a function of frequency (to 188 GHz) and temperatures down to 4 K on **Na_{12}-1** showed that the Mn_4 unit is strongly exchange-coupled, with a frequency above 188 GHz, since the spectra stay isotropic at $g = 1.9949 \pm 0.0008$. We were unable to explain the temperature and field dependence of its magnetization and await further theoretical development, as discussed in the text. EPR and magnetization measurements on **Na_{11}Cs-2** were fully consistent with its low-lying states consisting of two singlets ($S = 0$), three triplets ($S = 1$), and one quintet ($S = 2$). Table 3 provides the spin Hamiltonian parameters for both compounds, and their interpretation is consistent with the overall X-ray structures for polyoxoanions **1** and **2**.

Our work re-emphasizes that polyoxoanions are a unique class of compounds because (a) four isostructural germanotungstate derivatives (**1**−**4**) substituted by four different transition-metal ions were synthesized, (b) polyanions **1**−**4** have silico- and phosphotungstate analogues and therefore they represent a very large family of sandwich-type compounds which allows for comparative studies, (c) different hetero groups result in slight changes of bond lengths and angles and may also lead to different polyoxoanion charges (e.g., P vs Ge), (d) incorporation of different 3d transition-metal ions results in slight changes of bond lengths and angles because of different coordination requirements (e.g., Mn^{2+} vs Cu^{2+}), (e) it was also possible to incorporate 4*d* metals in the same polyoxoanion matrix and to study the structural effects, (f) the solid-state polyoxoanion structure is conserved in solution, which allows for homogeneous catalysis applications, (g) the four paramagnetic transition-metal ions are arranged as a rhombic M_4O_{16} metal-oxo cluster with spin-exchange coupling via bridging oxo-groups, (h) the magnetic metal-oxo cluster is structurally well-defined and surrounded by a diamagnetic tungsten-oxo framework, (i) the metal-oxo clusters of different polyoxoanions are well-isolated from each other so that intermolecular magnetic

phenomena are essentially negligible, and (j) the complexity due to the many magnetic (spin) exchange pathways render these compounds to be good examples of spin-frustrated systems. In this regard, the magnetization analysis of $\mathbf{Na_{12}}$**-1** has been less satisfactory and had to be postponed to future investigations.

Acknowledgment. The ^{183}W-NMR measurements were performed by P. Mayer (LMU) at the Ludwig Maximilians University Munich. X-ray measurements for polyanions **1**, **3**, and **4** were performed by U.K. during a visiting appointment at Georgetown University in the laboratory of Prof. M. T. Pope. X-ray measurements for polyanion **2** were performed by U.K. during a visit in the laboratory of Prof. N. Dalal (Florida State University). U.K. thanks both Chemistry Departments for allowing use of the X-ray diffractometer. We thank Dr. L. Bi for providing the nonatungstogermanate precursors. We also thank Dr. Hans van Tol (National High Magnetic Field Laboratory, Tallahassee) for helpful discussions. Figures 1 and 2 were generated by Diamond Version 2.1e (copyright Crystal Impact GbR).

Supporting Information Available: Ball and stick representations of the asymmetric units of **1**−**4** showing 50% probability ellipsoids and the labeling scheme and four X-ray crystallographic files in CIF format. This material is available free of charge via the Internet at http://pubs.acs.org.

IC0354421